Chinese Chemical Letters 34 (2023) 108383

Contents lists available at ScienceDirect

Chinese Chemical Letters

journal homepage: www.elsevier.com/locate/cclet

Wavelength-dependent three-dimensional single-molecule superlocalization imaging for yoctomole detection of thyroid-stimulating hormone on a quantum dot nanobiosensor

Junghwa Lee [a,1], Seungah Lee [b,1], Seong Ho Kang [a,b,*]

[a] Department of Chemistry, Graduate School, Kyung Hee University, Yongin-si, Gyeonggi-do 17104, Republic of Korea
[b] Department of Applied Chemistry and Institute of Natural Sciences, Kyung Hee University, Yongin-si, Gyeonggi-do 17104, Republic of Korea

ARTICLE INFO

Article history:
Received 12 January 2023
Revised 10 February 2023
Accepted 27 March 2023
Available online 30 March 2023

Keywords:
Single-molecule nanobiosensor
Thyroid stimulating hormone
Yoctomole detection
3D superlocalization
Imaging

ABSTRACT

A wavelength-dependent three-dimensional (3D) superlocalization imaging method on gold nanoislands (GNIs) chip was developed as a supersensitive single-molecule thyroid-stimulating hormone (TSH) nanobiosensor. Scattered and fluorescent signals from gold nanoislands on the substrate and quantum dots (QDs) nanoprobes were simultaneously isolated and acquired within an evanescent field layer generated by total internal reflection (TIR) of incident light using a dual-view device. The 3D TIR fluorescence images of TSH-bound QDs on the GNIs were obtained using *z*-axis optical sectioning at 10 nm intervals before/after immunoreaction to identify the optimal conditions for detection. The localized centroid position of QD nanoprobes and GNI were distinguished at a subdiffraction limit resolution using 3D Gaussian fitting to the point spread function. The QD TSH nanobiosensor using wavelength-dependent 3D TIR fluorescence-based single-molecule localization microscopy (3D TIRF-SLM) imaging technique showed an excellent detection limit of 90 yoctomoles (~54 molecules) and a wide linear dynamic range of 1.14 zmol/L – 100 pmol/L for TSH. The detection sensitivity was about 4.4×10^9 times higher than conventional enzyme-linked immunosorbent assay and could successfully quantify TSH in human serum. The wavelength-dependent 3D TIRF-SLM technique may emerge as a reliable platform for ultrahigh-sensitive nanobiosensors at the single-molecule level and early diagnosis with quantification of disease-related ultra-trace biomolecules.

Single-molecule nanobiosensors are powerful tools for observing interactions between individual molecules and the unique properties of molecular populations with high specificity and accuracy. Therefore, many researchers have focused on developing sensors with improved sensitivity and accuracy. Optical single-molecule immunosensors have some distinct advantages, like their ability to detect trace amounts of disease-related biomarkers and quantify them over a wide dynamic range [1]. Single-molecule optical immunosensors use labeled and unlabeled assays based on various platforms to achieve high sensitivity, selectivity, and localization [2,3]. However, the optical-based single-molecule immunosensors are limited by light diffraction and can only discriminate immunocomplexes from non-immunocomplex molecules at nanometer and spatiotemporal resolutions. We addressed this limitation by combining ultrahigh-resolution imaging and ultrasensitive optical immunosensors to measure molecular interactions and characterized antigen-antibody binding at the single-molecule level. A super-resolution imaging-based ultrasensitive optical immunosensor is required to overcome the diffraction limit of light [1–5].

Single-molecule localization microscopy (SLM) can be scaled for use beyond a diffraction-limited spatial resolution of about 200 nm. SLM can be used to analyze individual molecules with improved three-dimensional (3D) resolution and for quantitative measurements [6] like counting molecules [7], estimating stoichiometric variables [8], characterizing spatial distributions [9], and localizing with high-precision [10]. Recently, Kang and coworkers used 3D superlocalization-based immunoassay techniques to accurately quantify biomolecules by localizing limited nanoscale regions in the lateral and axial directions [11,12]. However, these techniques are limited by their inability to remove noise from the

* Corresponding author at: Department of Applied Chemistry and Institute of Natural Sciences, Kyung Hee University, Yongin-si, Gyeonggi-do 17104, Republic of Korea.
E-mail address: shkang@khu.ac.kr (S.H. Kang).
[1] These authors contributed equally to this work.

https://doi.org/10.1016/j.cclet.2023.108383
1001-8417/

dark-field microscopy light source [11] and the substrate's background (*i.e.*, the scattering signal of gold nanospots) [12].

We developed a supersensitive single-molecule thyroid-stimulating hormone (TSH) nanobiosensor using a total internal reflection (TIR) fluorescence-based wavelength-dependent superlocalization of quantum dot (QD) nanoprobe on gold nanoisland chips using 3D screening to identify optimum detection conditions and antigen-antibody molecular interactions (Fig. S1 in Supporting information). For the 3D screening, superlocalization images taken simultaneously with gold nanoisland (GNI) and QD at 10 nm *z*-spacing using a dual-view device in the optical path were reconstructed with a 3D Gaussian least-squares criterion algorithm to fit the point spread function and determine the locations of individual molecules at subdiffraction limit resolution (please see "Experiment procedures" section in Supporting information). This method was applied to both standard and real human blood samples (*i.e.*, serum), and its applicability was verified through comparison with the conventional enzyme-linked immunosorbent assay (ELISA) method.

Hyperspectral image (HSI), scanning electron microscopy (SEM), and atomic force microscopy (AFM) were used to confirm the presence or absence of TSH antigen-antibody molecular interactions on the GNI. In the HSI data, the intrinsic scattering color of the GNI array was orange, and the resonance scattering peak was around 601 nm (Fig. S2a in Supporting information). Compared with the extinction spectrum of only GNI, the resonance scattering peak of GNI was redshift (~639 nm, white color) after the sandwich immunoreaction of TSH-QD (11 fmol/L) (Fig. S2b in Supporting information). In the SEM data, white spots were observed on the GNI after the reaction that occurred on a clean GNI before the TSH reaction (Figs. S3a and c in Supporting information). The sequence immunoassays for GNI were GNI, DSP linker, protein A/G, primary antibody, TSH antigen, biotinylated antibody, and streptavidin-QD. The average height of a 300 nm GNI was approximately 14.5 nm and 0.6 nm for DSP. Protein A/G consisted of 5 nm for protein A and 1.4 nm for protein G. We used 14.5 nm for the primary antibody, 4.0–6.5 nm for the TSH antigen, 14.5 nm for the second antibody, and 20 nm QD. Therefore, the theoretical total height of the sandwich immunoreaction to GNI was about >79.6 nm [13]. However, the experimental AFM data differed from the theoretical height value since 20 nm QD nanoprobes can be placed in random axial and lateral locations on a GNI within a limited area (Figs. S3b and d in Supporting information). Moreover, organic linkers used for the immunoreaction are flexible and inconsistently oriented along the vertical *z*-axis [14,15]. These results demonstrate successful TSH antigen-antibody reaction on the GNI substrate.

We confirmed the presence or absence of non-specific binding and cross-reaction using the fluorescence signal after immunoreaction with (a) a positive control using 100 pmol/L of the target molecule (TSH), (b) the absent target molecule, and (c) a negative control using T3 antigen (Fig. S4 in Supporting information). Here, in the TSH antigen-antibody reaction in Fig. S4a, a fluorescence signal was detected; however, no fluorescence signal was detected when the antibody was absent or when the non-corresponding antigen T3 was reacted. This result shows that the fluorescence signal detected by the TSH nanobiosensor chip can ignore non-specific binding or cross-reaction.

The wavelength-dependent 3D TIR fluorescence-based single-molecule localization microscopy (3D TIRF-SLM) system simultaneously provided signals from QDs (nanoprobes) and the GNI on a single screen for two-dimensional (2D) localization of TSH molecules on the GNI (Figs. 1a and b). The raw images collected through the 3D TIRF-SLM system were reconstructed into 3D images using the least cubic algorithm (within the supplementary information). The target TSH molecules immunoreacted onto the GNI could be superlocalized by calculating the *x*-, *y*-

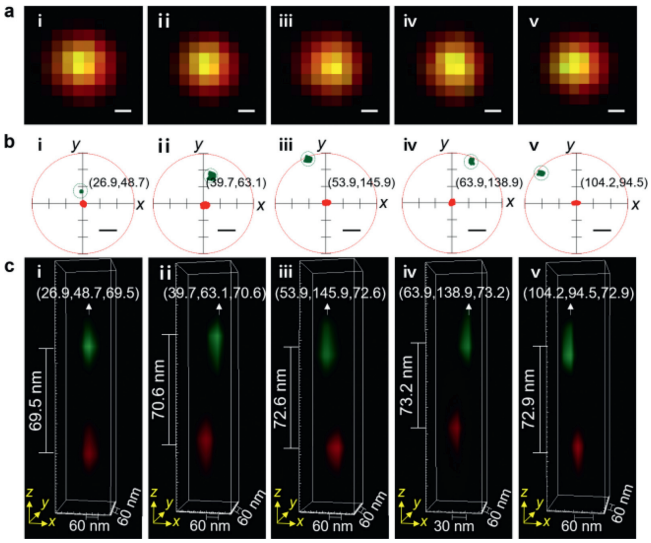

Fig. 1. (a) Raw TIRF images of five individual QD nanoprobes on GNIs after the TSH sandwich immunoreaction. (b) Reconstructed wavelength-dependent 2D superlocalization and *x*, *y* coordinates of QD nanoprobes on GNIs. (c) On a TSH biochip, reconstructed wavelength-dependent 3D TIRF-SLM images of QD nanoprobes (green) and GNIs (red). The theoretical axial distance difference between GNI and QD is about >79.6 nm. The numbers in parentheses indicate the coordinates of the nanoprobe after fixing the GNI to the coordinates of (0, 0). The concentration of standard TSH is 1.3 fmol/L. Scare bar = 100 nm.

and *z*-direction distances between the 300 nm GNI and the 20 nm QD (Fig. 1c). Fig. 1a shows raw, 2D TIRF images from five sample cases. Fig. 1b shows the 2D localization images computed by 2D Gaussian fitting of the exact centroids of QD nanoprobes and GNIs of the five sample cases. Fig. 1c shows the 3D reconstruction of the five sample cases. The superlocalization results of pre-reaction TIRF-SLM images showed no central pre-reaction changes ($d_c = \Delta x = \Delta y = \Delta z = 0$). After the reaction of representative sample "i," the relative coordinates of the QDs along the *x*, *y*, and *z* directions of the 3D superlocalized TIRF-SLM image were $\Delta x = 26.9$, $\Delta y = 48.7$ and $\Delta z = 69.5$ nm (Fig. 1c(i)). The relative coordinates of *x*, *y*, *z*, and the center differences distance (d_c) of GNI and QD for the five samples are shown in Table S1 (Supporting information). This clearly depicts 3D superlocalization of random nanoprobe (*e.g.*, 20 nm QD) distribution by TSH antigen-antibody immunoreactivity in a confined area (*e.g.*, 300 nm GNI).

Sensitive measures of trace amounts of serum TSH are used for thyroid testing, with increased TSH levels generally representing diminished thyroid hormone production. Depending on urgency of diagnosis, the ultra-sensitivity to serum TSH should be measured [16,17]. We compared a commercially available ELISA kit and 3D TIRF-SLM using quantitative calibration curves and increasing TSH concentrations *vs.* absorption and fluorescence signals (Fig. 2). The 3D fluorescence intensity plot indicated that the fluorescence intensity decreased with decreasing TSH concentrations (Fig. 2c). The 3D TIRF-SLM method was very sensitive and featured a wide linear dynamic range of 1.14 zmol/L and 100 pmol/L (correlation coefficient, $R^2 = 0.996$) under 473 nm laser illumination (Fig. 2a). In addition, the TSH limit of detection (LOD) was 90 yoctomole, $\sim 4.4 \times 10^9$ times lower than the LOD of 0.4 pmol/L obtained by conventional ELISA (3–200 pmol/L, $R^2 = 0.993$) (Fig. 2b), and 4×10^3 times lower than the previously reported TIRF detection method with a wide dynamic range (360 zmol/L – 36 pmol/L) [18]. The sensitivity of the 3D TIRF-SLM method surpasses other TSH detection methods such as surface-enhanced Raman spectroscopy-lateral flow immunoassay (SERS-LFIA) [19], lab-on-a-chip (LOC) [20], 1,1′-oxalyldiimidazole chemilu-

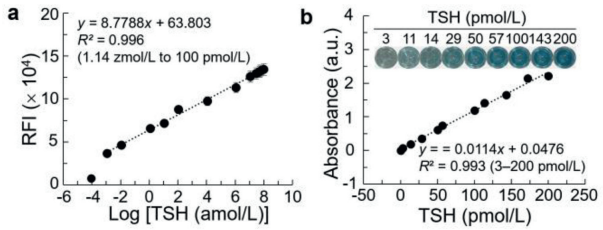

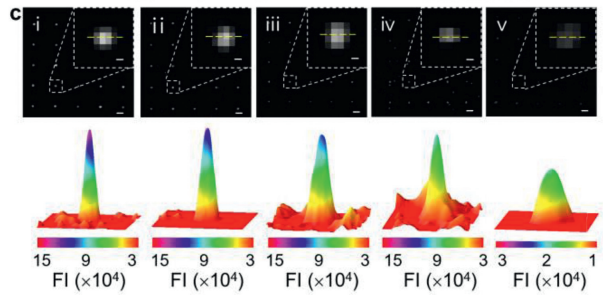

d

TSH conc. (pmol/L)	Mean conc. (pmol/L)		Difference
	3D TIRF-SLM	ELISA	
100	102.33	99.37	-2.96
57	60.26	61.11	0.86
50	52.48	49.38	-3.09
29	29.99	28.37	-1.62
10	10.05	11.29	1.24
		$\lvert\bar{d}\rvert$ =	1.12
		S_d =	2.06
		$t_{calculated}$ =	1.08

Fig. 2. (a) Quantitative calibration curves of standard TSH over a wide dynamic range of 1.14 zmol/L to 100 pmol/L by 3D TIRF-SLM. (b) Standard calibration curve and ELISA images (inner) of the TSH sandwich reaction obtained using a commercially available ELISA kit. (c) TIRF raw images of target TSH molecules in samples as a function of concentration following a sandwich immunoreaction and RFI values in 3D plots as a function. (d) Paired *t*-test for TSH validation of 3D TIRF-SLM method compared with the ELISA method. Comparing *t*-test values to the *t*-table, *t* values less than 3.747 in the *t*-table at the 98% confidence level (Table S2 in Supporting information). c(i)–c(v) represents 11.4 pmol/L, 11.4 fmol/L, 11.4 amol/L, 11.4 zmol/L, and 1.14 zmol/L, respectively; Scare bar = 1 μm (inner = 100 nm); LOD, limit of detection; a.u. = arbitrary unit; RFI, relative fluorescence intensity.

minescence (ODI-CL) [21], lateral flow [22], ODI-chemiluminescent enzyme immune assay (CLEIA) [23], and LFIA [24]. The details of several TSH detection methods, including detection limits and dynamic linear ranges, are summarized in Table 1.

Our novel method was additionally verified by comparing various TSH concentrations (*i.e.*, 10, 29, 50, 57, and 100 pmol/L) with the ELISA method. The difference between the two methods was determined using paired Student's *t*-test. "Difference" in Fig. 2d represents the difference ($|\bar{d}|$) between two results obtained from standard samples. The calculated difference means ($|\bar{d}|$) and standard deviation (S_d) of the five differences were 1.12 and 2.06, respectively. The value of $t_{calculated}$ (t_{cal}) was calculated according to the formula:

$$t_{cal} = \left(\frac{|\bar{d}|}{s_d}\right)(n)^{1/2} = 1.08$$

where $|\bar{d}|$ is the absolute value of the average difference. Here, the t_{cal} (1.08) < t_{table} (3.747) with 98% confidence and 4 degrees of freedom. Therefore, the two methods were significantly different the 98% confidence level. These results indicate the feasibility of 3D TIRF-SLM for detecting and quantifying TSH (Fig. 2).

To confirm the applicability of using this method with human serum samples, standard TSH samples were spiked into two

Table 1
Comparison of dynamic linear ranges and LODs using various TSH detection methods.

Method[a]	Linear dynamic range (mol/L)	LOD[b] (mol/L)	Ref.
SERS-LFIA	–	143×10^{-9}	[19]
EC	4.56×10^{-14}–9.12×10^{-11}	2.28×10^{-14}	[16]
LOC	314.60×10^{-12}	10.87×10^{-12}	[20]
ODI-CL	0.21–102.96×10^{-12}	0.06×10^{-12}	[21]
Lateral flow	0.10–171.60×10^{-12}	0.10×10^{-12}	[22]
ODI CLEIA	0.07–68.64×10^{-9}	0.03×10^{-9}	[23]
LFIA	1.43–28.60×10^{-12}	0.11×10^{-12}	[24]
TIRFM	360×10^{-18}–36×10^{-9}	360×10^{-21}	[18]
ELISA	$3 - 200 \times 10^{-12}$	0.4×10^{-12}	This work
3D TIRF-SLM	1.14×10^{-21}–100×10^{-12}	90×10^{-24}	This work

[a] Abbreviations: SERS, surface-enhanced Raman spectroscopy; EC, electrochemical; LOC, lab-on-a-chip; ODI-CL, 1,1′-oxalyldiimidazole chemiluminescence; ODI CLEIA, 1,1′-oxalyldiimidazole chemiluminescent enzyme immune assay; LFIA, lateral flow immunoassay; TIRFM, total internal reflection fluorescence microscopy; ELISA, enzyme-linked immunosorbent assay; 3D TIRF-SLM, three-dimensional TIRF microscopy based on superlocalization microscopy.
[b] LOD, limit of detection (S/N = 3).

healthy human serum (human type AB male) samples with different concentrations (*i.e.*, 5 pmol/L and 10 pmol/L). The concentration of spiked TSH in human serum sample was determined by the 3D TIRF-SLM and ELSIA at 8.17 pmol/L and 8.50 pmol/L, respectively (Fig. 3). Thus, the wavelength-dependent 3D TIRF-SLM method can analyze various disease-related biomarkers in human serum samples with high sensitivity and reliability at the single-molecule level.

We developed a wavelength-dependent 3D TIRF-SLM method for single TSH molecule detection and quantification with a wide dynamic linear range on a QD nanobiosensor chip. The superlocalization of the nanoscale region to the GNI and TSH-bound QDs was coordinated by 3D Gaussian fitting at the single-molecule level. The biomolecule's axial height was selectively measured using the *z*-axis cross-section of the QD nanoprobe. GNI intensity and individual antigen-antibody interactions and binding were confirmed by calculating the central location distribution region. The quantitative immunoassay of TSH molecules had a wide dynamic linear range of 1.14 zmol/L to 100 pmol/L ($R^2 = 0.996$) and a LOD of 90 yoctomole (~54 molecules). In addition, a *t*-test compared the method developed using the ELISA kit with healthy human serum samples showed 98% significance, proving its successful application. Therefore, the 3D TIRF-SLM method overcomes the limitations

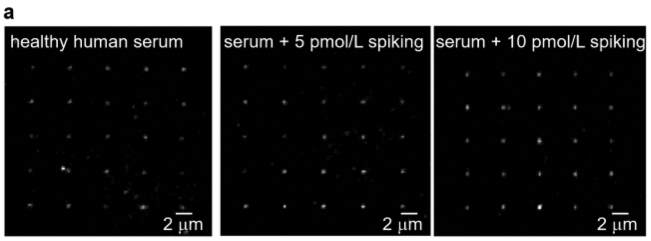

b

Sample	TSH concentration (pmol/L)	
	3D TIRF-SLM	ELISA
Healthy human serum	8.165 ± 0.261[a]	8.504 ± 0.074[a]
Seurm + TSH 5 pmol/L spiking	14.321 ± 0.377[a]	13.523 ± 0.083[a]
Seurm + TSH 10 pmo/L spiking	19.091 ± 0.935[a]	18.411 ± 0.058[a]

Fig. 3. (a) Raw TIRF images obtained using the 3D TIRF-SLM method after immunoreaction with healthy human serum (left) and serum samples spiked with 5 pmol/L and 10 pmol/L standard TSH (middle and right). (b) Table comparing the quantification of TSH spiked serum samples using 3D TIRF-SLM and ELISA methods based on the calibration curves in Figs. 2a and b. [a] Mean ± SD (mean ± standard deviation, $n = 3$).

of detection sensitivity and selectivity of the existing single biosensor methods by combining the excellent photostability, high sensitivity, and superlocalization of QD nanoprobes on GNIs and a 3D super-resolution imaging method within an evanescent field layer. This method may emerge as a reliable platform with the ability to directly detect various disease-associated biomarkers in human biological samples at the single-molecule level by altering the antibody in the target molecule.

Declaration of competing interest

The authors declare no competing financial interests.

Acknowledgments

This work was supported by the National Research Foundation of Korea (NRF) grant funded by the Korea government (MSIT) (Nos. 2019R1A2C2002556 and 2020R1C1C1009668). This research was supported by Nano-Material Technology Development Program through the NRF funded by the Ministry of Science, ICT and Future Planning (No. 2009–0082580).

Supplementary materials

Supplementary material associated with this article can be found, in the online version, at doi:10.1016/j.cclet.2023.108383.

References

[1] N. Akkilic, S. Geschwindner, F. Höök, Biosens. Bioelectron. 151 (2020) 111944.
[2] Y. Liu, B. Li, B. Liu, K. Zhang, Biosens. Basel 12 (2022) 1105.
[3] S. Lee, J. Lee, Y. Cao, C. An, S.H. Kang, Biosens. Bioelectron.: X 11 (2022) 100191.
[4] S.O. Kelley, ACS Sens. 2 (2017) 193–197.
[5] F. Karim, T.B. Smith, C. Zhao, J. Nanophotonics 12 (2017) 012504.
[6] A. Shivanandan, H. Deschout, M. Scarselli, A. Radenovic, FEBS Lett. 588 (2014) 3595–3602.
[7] D. Lando, U. Endesfelder, H. Berger, et al., Open Biol. 2 (2012) 120078.
[8] J. Gunzenhäuser, N. Olivier, T. Pengo, S. Manley, Nano Lett. 12 (2012) 4705–4710.
[9] J. Rossy, D.M. Owen, D.J. Williamson, Z. Yang, K. Gaus, Nat. Immunol. 14 (2013) 82–89.
[10] A. Szymborska, A. de Marco, N. Daigle, et al., Science 341 (2013) 655–658.
[11] S. Ju, S. Lee, S.K. Chakkarapani, et al., Anal. Chem. 90 (2018) 5100–5107.
[12] S.K. Chakkarapani, Y. Sun, S.H. Kang, Sens. Actuator. B: Chem. 284 (2019) 81–90.
[13] S. Lee, J. Lee, I. Batjikh, H. Yu, S.H. Kang, ACS Sens. 7 (2022) 1372–1380.
[14] S. Ahn, P. Zhang, H. Yu, S. Lee, S.H. Kang, Anal. Chem. 88 (2016) 11070–11076.
[15] S. Ju, S. Lee, S.K. Chakkarapani, et al., Anal. Chem. 90 (2018) 5100–5107.
[16] Y. Cui, H. Chen, L. Hou, et al., Anal. Chim. Acta 738 (2012) 76–84.
[17] J. Lee, S. Lee, G. Lee, S.H. Kang, Biosens. Bioelectron. 220 (2023) 114894.
[18] S. Lee, S.H. Kang, Talanta 99 (2012) 1030–1034.
[19] S. Choi, J. Hwang, S. Lee, et al., Sens. Actuator. B: Chem. 240 (2017) 358–364.
[20] W. Jung, J. Han, J. Kai, et al., Lab Chip 13 (2013) 4653–4662.
[21] C. Shim, R. Chong, J.H. Lee, Talanta 171 (2017) 229–235.
[22] S.L. Znoyko, A.V. Orlov, V.A. Bragina, M.P. Nikitin, P.I. Nikitin, Talanta 216 (2020) 120961.
[23] G. Choi, E. Kim, E. Park, J.H. Lee, Talanta 162 (2017) 38–45.
[24] P. Preechakasedkit, K. Osada, Y. Katayama, et al., Analyst 143 (2018) 564–570.